

# Summary

|    |   |  |           |
|----|---|--|-----------|
| 2  | <b>1</b>  | <b>Introduction</b>  | <b>2</b>  |
| 3  | <b>2</b>  | <b>Pixel detectors</b>   | <b>3</b>  |
| 4  | 2.1   | Signal formation . . . . .   | 3         |
| 5  | 2.2   | Hybrid pixels . . . . .  | 4         |
| 6  | 2.3   | CMOS MAPS and DMPAS . . . . .                                      | 5         |
| 7  | 2.3.1   | DMAPS: large and small fill factor . . . . .                       | 5         |
| 8  | 2.3.2   | A modified sensor . . . . .  | 6         |
| 9  | 2.4   | Analog front end . . . . .   | 7         |
| 10 | 2.4.1   | Preamplifier . . . . .   | 8         |
| 11 | 2.5   | Readout logic . . . . .  | 8         |
| 12 | <b>3</b>  | <b>Use of pixels detector</b>                                      | <b>11</b> |
| 13 | 3.1   | Tracking in HEP . . . . .  | 11        |
| 14 | 3.1.1   | Hybrid pixels: ATLAS, CMS and LHC-b . . . . .                      | 11        |
| 15 | 3.1.2   | CMOS MAPS: ALICE and STAR . . . . .                                | 11        |
| 16 | 3.2   | Application in medical imaging . . . . .                           | 11        |
| 17 | 3.2.1   | Medipix and Timepix . . . . .                                      | 11        |
| 18 | 3.2.2   | Applicability to FLASH radiotherapy . . . . .                      | 11        |
| 19 | <b>4</b>  | <b>TJ-Monopix1</b>   | <b>12</b> |
| 20 | 4.1   | The sensor . . . . .   | 13        |
| 21 | 4.2   | FE flavors . . . . .   | 14        |
| 22 | 4.2.1   | ALPIDE-like front end . . . . .                                    | 14        |
| 23 | 4.2.2   | FE parameters . . . . .  | 15        |
| 24 | 4.3   | Readout logic . . . . .  | 15        |
| 25 | 4.3.1   | Dead time measurement . . . . .                                    | 18        |
| 26 | <b>5</b>  | <b>Arcadia-MD1</b>   | <b>19</b> |
| 27 | 5.1   | The sensor . . . . .   | 19        |
| 28 | 5.2   | Readout logic and data structure . . . . .                         | 19        |
| 29 | 5.2.1   | Matrix division and data-packets . . . . .                         | 19        |
| 30 | <b>6</b>  | <b>Threshold and noise characterization</b>                        | <b>23</b> |
| 31 | 6.1   | Threshold and noise: figure of merit for pixel detectors . . . . . | 23        |
| 32 | 6.2   | TJ-Monopix1 characterization . . . . .                             | 24        |
| 33 | 6.3   | ARCADIA-MD1 characterization . . . . .                             | 24        |
| 34 | <b>A</b>  | <b>Pixels detector: a brief overview</b>                           | <b>25</b> |
| 35 | A.1   | Radiation damages . . . . .  | 25        |
| 36 | <b>B</b>  | <b>FLASH radiotherapy</b>  | <b>27</b> |
| 37 | B.1   | Cell survival curves . . . . .                                     | 27        |
| 38 | B.2   | FLASH effect . . . . .   | 28        |
| 39 | <b>Bibliography</b>   |  | <b>29</b> |
| 40 | Characterization of monolithic CMOS pixel sensors for charged particle detectors and for high intensity dosimetry |  |           |
| 41 |   |  |           |

<sup>42</sup> **Chapter 1**

<sup>43</sup> **Introduction**

<sup>44</sup> Pixel detectors, members of the semiconductor detector family, have significantly been used since  
<sup>45</sup> () at the first accelerator experiments for energy and position measurement. Because of their  
<sup>46</sup> dimension (today  $\sim 30 \mu m$  or even better) and their spatial resolution ( $\sim 5\text{-}10 \mu m$ ), with the  
<sup>47</sup> availability of technology in 1980s they proved to be perfectly suitable for vertex detector in the  
<sup>48</sup> inner layer of the detector.

<sup>49</sup> Technological development has been constant from then on and today almost every high energy  
<sup>50</sup> physics (HEP) experiment employs a pixels detector; hybrid pixel currently constitute the state-  
<sup>51</sup> of-art for large scale pixel detector but experiments began to look at the more innovative monolithic  
<sup>52</sup> active pixels (MAPS) as perspective for their future upgrades, as BelleII, or they already have  
<sup>53</sup> installed them, as ALICE.

<sup>54</sup> Requirement imposed by accelerator are stringent and they will be even more with the increase  
<sup>55</sup> of luminosity/intensity, in terms of radiation hardness, efficiency and occupancy, time resolution,  
<sup>56</sup> material budget and power consumption.

<sup>57</sup> Qual è invece la richiesta per la dosimetria?

<sup>58</sup>

<sup>59</sup> **Chapter 2**

<sup>60</sup> **Pixel detectors**

<sup>61</sup> **2.1 Signal formation**

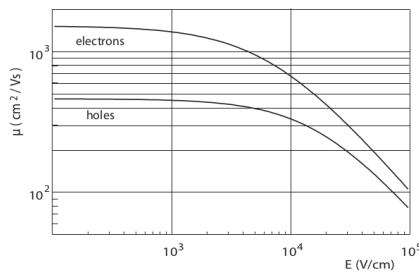
<sup>62</sup> When a charge particle passes through a pixel and loses energy by ionization a part of that  
<sup>63</sup> energy is used to generate electron-hole pairs (another part is used for other processes, as the  
<sup>64</sup> lattice excitation) which are then separated by the electric field and collected at their respectively  
<sup>65</sup> electrodes ( $p$  for holes and  $n$  for electrons)<sup>1</sup>; by the drift of these charges, a signal  $i_e$  is generated  
<sup>66</sup> on the electrode  $e$  as stated by the Shockley–Ramo's theorem:

$$i_e(t) = -q v(t) E_{WF,e} \quad (2.1)$$

<sup>67</sup> where  $v(t)$  is the instantaneous velocity of the charge  $q$  and  $E_{WF}$  is the weighting field, that is the  
<sup>68</sup> field obtained biasing the electrode  $e$  with 1V and all the others with 0V. The drift velocity of the  
<sup>69</sup> charge depends on the electric field and on the mobility of the particle:

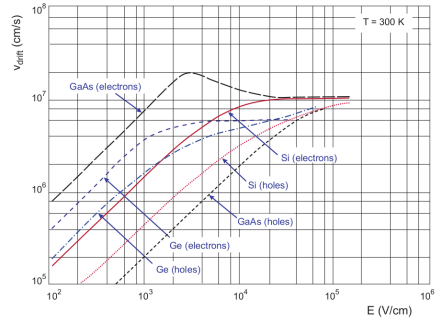
$$v = \mu(E) E \quad (2.2)$$

<sup>70</sup> where  $\mu(E)$  is a function of the electric field and is linear with  $E$  only for small  $E$ : at higher values  
<sup>71</sup> the probability of interactions with optical phonons increases and the mobility drops and this leads  
<sup>72</sup> to an independence of the velocity from the electric field (fig. 2.1b).



(a) Typical values for electrons and holes mobility in

silicon at room temperature are  $\mu_n \sim 1450 \text{ cm}^2/\text{Vs}$ ,  $\mu_h = 500$



(b) Drift velocity at room temperature in different semiconductors

<sup>73</sup> The average energy needed to create a pair at 300 K in silicon is  $w_i = 3.65 \text{ eV}$ , that is more  
<sup>74</sup> than the mean ionization energy because of the interactions with phonon, since for a minimum  
<sup>75</sup> ionizing particle (MIP) the most probable value (MPV) of charge released in the semiconductor is  
<sup>76</sup> 0.28 keV/ $\mu$ , hence the number of e/h pairs is:

$$\langle \frac{dE}{dx} \rangle \frac{1}{w_i} \sim 80 \text{ e}/\text{h} \sim \frac{1.28 \cdot 10^{-2} fC}{\mu m} \quad (2.3)$$

<sup>1</sup>Even if in principle both the electrode can be used to read a signal, for pixel detectors, where the number of channel and the complexity of readout are high, only one is actually used. In strip and pad detectors, instead, is more common a dual-side readout

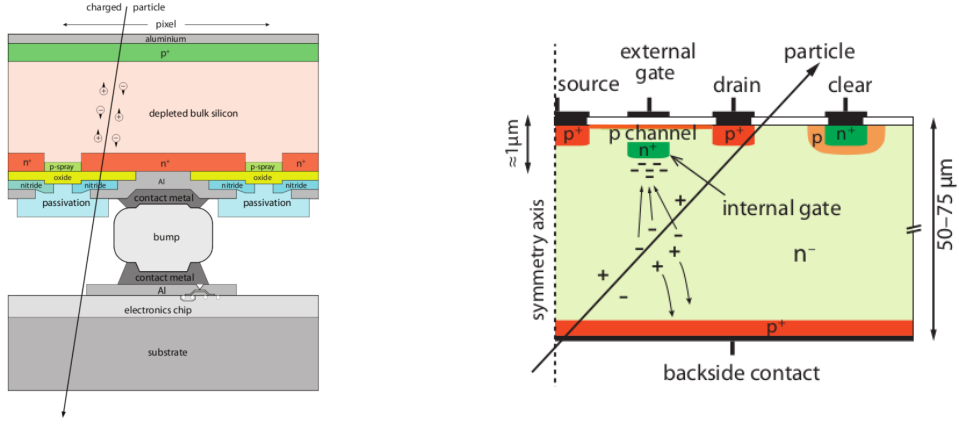


Figure 2.2: Concept cross-section of hybrid pixel (a) and of a DEPFET (b)

77 CON UN'INCERTEZZA CHE È RADICE DI N; ED EVENTUALEMTE SI AGGIUNGE IL  
 78 FATTORE DI FANO NEL CASO DI ASSORBIMENTO TOTALE. IL FATTORE DI FANO È  
 79 0.115 NELL SILICIO. ecc It is fundamental that pairs e/h are produced in the depleted region  
 80 of the semiconductor where the probability of recombination with charge carriers is low to avoid  
 81 loss of signals. Pixel detectors are then commonly reverse biased: a positive bias is given to the  
 82 n electrode and a negative to the p to grow the depletion zone in the epitaxial layer below the  
 83 electrode. The width of the depletion region is related with the external bias  $V_{ext}$ , the resistivity  
 84  $\rho$  and also with the dopant:

$$d_n \sim 0.55 \sqrt{\frac{\rho}{\Omega cm} \frac{V_{ext}}{V}} \mu m \quad (2.4) \quad d_p \sim 0.32 \sqrt{\frac{\rho}{\Omega cm} \frac{V_{ext}}{V}} \mu m \quad (2.5)$$

85

86

87

88 For that reason high resistivity wafers ( $100 \Omega cm - k\Omega cm$ ) are typically preferred because they  
 89 allow bigger depletion zone with smaller voltage bias.

## 90 2.2 Hybrid pixels

91 Hybrid pixels are made of two parts (fig. 2.2a), the sensor and the electronics: for each pixel these  
 92 two parts are welded together through microconnection (bump bond).  
 93 They provide a practical system where readout and sensor can be optimized separately, although  
 94 the testing is less easy-to-do since the sensor and the R/O must be connected together before.  
 95 In addition, the particular and sophisticated procedure to bond sensor and ASIC (application spe-  
 96 cific integrated circuit) makes them difficult to produce, delicate, especially when exposed to high  
 97 levels of radiation, and also expensive.  
 98 A critical parameter for accelerator experiments is the material budget, which represents the main  
 99 limit factor for momentum measurement resolution in a magnetic field; since hybrid pixels are  
 100 thicker ( $\sim$  hundreds of  $\mu m$ ) than monolithic ones (even less than  $100 \mu m$ ), using the latter the  
 101 material budget can be down by a third: typical value for hybrid pixels is 1.5 %  $X_0$  per layer,  
 102 while for monolithic 0.5 %  $X_0$ .  
 103 Among other disadvantages of hybrid pixels there is the bigger power consumption that implies,  
 104 by the way, a bigger cooling system leading in turn to an increase in material too.

105

106 DEPFET are the first attempt towards the integration of the front end (FE) on the sensor bulk:  
 107 they are typically mounted on a hybrid structure but they also integrate the first amplification  
 108 stage.

109 Each pixel implements a MOSFET (metal-oxide-semiconductor field-effect transistor) transistor  
 110 (a p-channel in fig. 2.2b): an hole current flows from source to drain which is controlled by the  
 111 external gate and the internal gate together. The internal gate is made by a deep n+ implant  
 112 towards which electrons drift after being created in the depletion region (to know how the signal

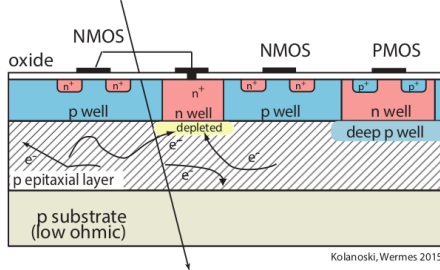


Figure 2.3: Concept cross-section of CMOS MPAS pixel

is created in a pixel detector look at appendix A); the accumulation of electrons in the region underneath the n implant changes the gate potential and controls the transistor current.  
DEPFET typically have a good S/N ratio: this is principally due the amplification on-pixel and the large depletion region. But, since they need to be connected with ASIC the limiting factor still is the material budget.

## 2.3 CMOS MAPS and DMPAS

Monolithic active pixels accommodate on the same wafer both the sensor and the front end electronics, with the second one implanted on top.

MAPS have been first proposed and realized in the 1990s and their usage has been enabled by the development of the electronic sector which guarantees the decrease in CMOS transistors dimension at least every two years, as stated by the Moore's law<sup>2</sup>.

As a matter of fact the dimension of components, their organization on the pixel area and logic density are important issues for the design and for the layout; typically different decisions are taken for different purposes.

Monolithic active pixel can be distinguished between two main categories: MAPS and depleted MAPS (DMAPS).

MAPS (figure a 2.3) have typically an epitaxial layer in range 1-20  $\mu\text{m}$  and because they are not depleted, the charge is mainly collected by diffusion rather than by drift. This makes the path of charges created in the bulk longer than usual, therefore they are slow (of order of 100 ns) and the collection could be partial especially after the irradiation of the detector (look at A for radiation damages), when the trapping probability become higher.

In figure 2.3 is shown as example of CMOS MAPS: the sensor in the scheme implements an n well as collection diode; to avoid the others n wells (which contain PMOS transistor) of the electronic circuit would compete in charge collection and to shield the CMOS circuit from the substrate, additionally underlying deep p well are needed. DMAPS are instead MAPS depleted with  $d$  typically in  $\sim 25\text{-}150 \mu\text{m}$  (eq. 2.1) which extends from the diode to the deep p-well, and sometimes also to the backside (in this case if one wants to collect the signal also on this electrode, additional process must be done).

### 2.3.1 DMAPS: large and small fill factor

There are two different sensor-design approaches (figure 2.4) to DMAPS:

- large fill factor: a large collection electrode that is a large deep n-well and that host the embedded electronics
- small fill factor: a small n-well is used as charge collection node

To implement a uniform and stronger electric field, DMAPS often uses large electrode design that requires multiple wells (typically four including deep n and p wells); this layout adds on to the standard terms of the total capacity of the sensor a new term (fig. 2.5), that contributes to the total amplifier input capacity. In addition to the capacity between pixels ( $C_{pp}$ ) and between the pixel and the backside ( $C_b$ ), a non-negligible contribution comes from the capacities between wells

<sup>2</sup>Moore's law states that logic density doubles every two years.

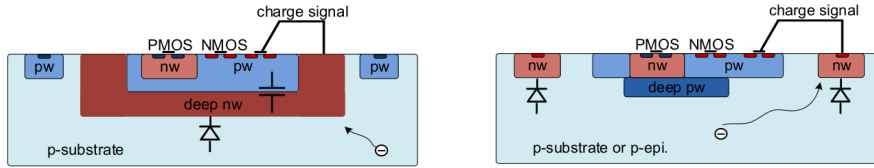


Figure 2.4: Concept cross-section with large and small fill factor

|                       | small fill factor | large fill factor |
|-----------------------|-------------------|-------------------|
| small sensor C        | ✓ (< 5 fF)        | ✗ (~ 100-200 fF)  |
| low noise             | ✓                 | ✗                 |
| low cross talk        | ✓                 | ✗                 |
| velocity performances | ✓                 | ✗ (~ 100 ns)      |
| short drift paths     | ✗                 | ✓                 |
| radiation hard        | ✗                 | ✓                 |

Table 2.1: Small and large fill factor DMAPS characteristics

151 ( $C_{SW}$  and  $C_{WW}$ ) needed to shield the embedded electronics. These capacities affect the thermal  
152 and 1/f noise of the charge amplifier and the  $\tau_{CSA}$  too:

$$ENC_{thermal}^2 \propto \frac{4}{3} \frac{kT}{g_m} \frac{C_D^2}{\tau_{sh}} \quad (2.6) \quad \tau_{CSA} \propto \frac{1}{g_m} \frac{C_D}{C_f} \quad (2.7)$$

154 where  $g_m$  is the transconductance,  $\tau_{sh}$  is the shaping time.  
155 Among the disadvantages coming from this large input capacity could be the coupling between  
156 the sensor and the electronics resulting in cross talk: noise induced by a signal on neighbouring  
157 electrodes; indeed, since digital switching in the FE electronics do a lot of oscillations, this problem  
is especially connected with the intra wells capacities. So, larger charge collection electrode

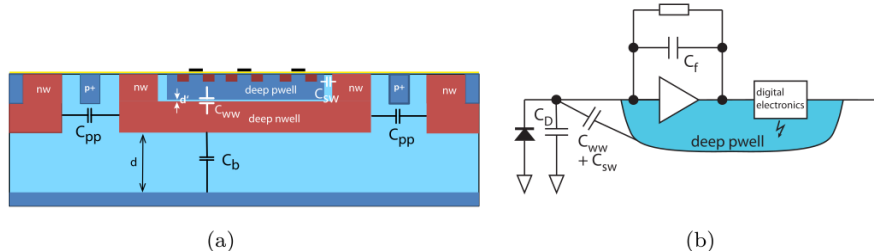


Figure 2.5:  $C_{pp}$ ,  $C_b$ ,  $C_{WW}$ ,  $C_{SW}$

158 sensors provide a uniform electric field in the bulk that results in short drift path and so in good  
159 collection properties, especially after irradiation, when trapping probability can become an issue.  
160 The drawback of a large fill-factor is the large capacity (~100 fF): this contributes to the noise  
161 and to a speed penalty and to a larger possibility of cross talk.

162 The small fill-factor variant, instead, benefits from a small capacity (5-20 fF), but suffers from  
163 a not uniform electric field and from all the issue related to that. **Ho già detto prima parlando dei  
164 MAPS, devo ripetere qui?**

165 As we'll see these two different types of sensor require different amplifier: the large electrode one is  
166 coupled with the charge sensitive amplifier, while the small one with voltage amplifier (sec 2.4.1).  
167

### 168 2.3.2 A modified sensor

169 ?? A process modification developed by CERN in collaboration with the foundries has become the  
170 standard solution to combine the characteristics of a small fill factor sensor (small input amplifier  
171 capacity) and of large fill factor sensor (uniform electric field) is the one carried out for ALICE

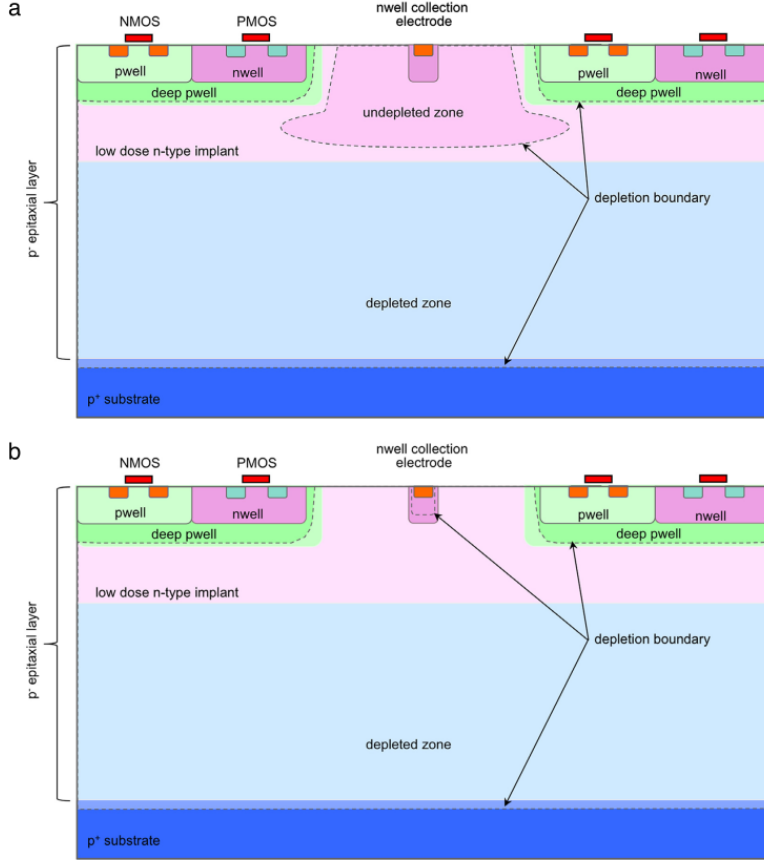


Figure 2.6: A modified process for ALICE tracker detector: a low dose n implant is used to create a planar junction. In (a) the depletion is partial, while in (b) the pixel is fully depleted.

172 upgrade about ten years [1].

173 A compromise between the two sensors could also be making smaller pixels, but this solution  
174 requires reducing the electronic circuit area, so a completely new pixel layout should be though.  
175 The modification consists in inserting a low dose implant under the electrode and one its advantage  
176 lies in its versatility: both standard and modified sensor are often produced for testing in fact.

177 Before the process modification the depletion region extends below the diode towards the sub-  
178 strate, and it doesn't extend laterally so much even if a high bias is applied to the sensor (fig. 2.6).

179 After, two distinct pn junctions are built: one between the deep p well and the  $n^-$  layer, and the  
180 other between the  $n^-$  and the  $p^-$  epitaxial layer, extending to the all area of the sensor.

181 Since deep p well and the p-substrate are separated by the depletion region, the two p electrodes  
182 can be biased separately<sup>3</sup> and this is beneficial to enhance the vertical electric field component.

183 The doping concentration is a trimmer parameter: it must be high enough to be greater than the  
184 epitaxial layer to prevent the punchthrough between p-well and the substrate, but it must also be  
185 lower enough to allow the depletion without reaching too high bias.

## 186 2.4 Analog front end

187 After the creation of a signal on the electrode, the signal enters the front end circuit (fig.2.7), ready  
188 to be molded and transmitted out of chip. Low noise amplification, fast hit discrimination and an  
189 efficient, high-speed readout architecture, consuming as low power as possible must be provided  
190 by the readout integrated electronics (ROIC).

191 Let's take a look to the main steps of the analog front end chain: the preamplifier (that actually  
192 often is the only amplification stage) with a reset to the baseline mechanism and a leakage current

---

<sup>3</sup>This is true in general, but it can be denied if other doping characteristics are implemented, and we'll see that this is the case of TJ-Monopix1

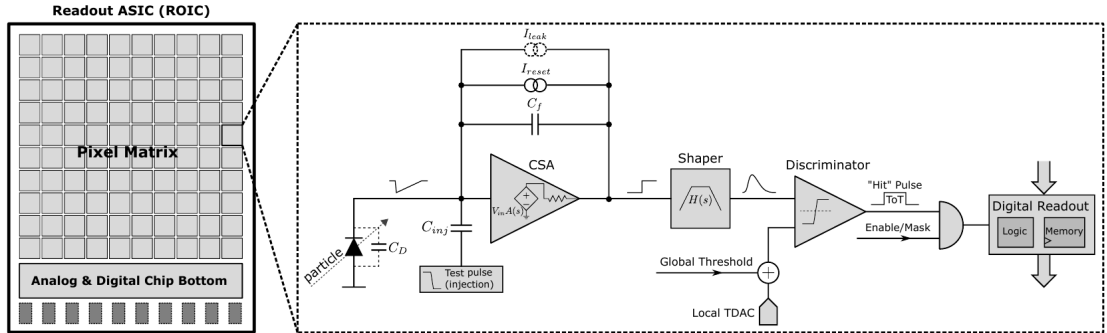


Figure 2.7: Readout FE scheme: in this example the preamplifier is a charge sensitive one (CSA) but changing the capacitive feedback into a resistive one, this can be converted in a voltage or current amplifier.

compensation, a shaper (a band-pass filter) and finally a discriminator. The whole chain must be optimized and tuned to improve the S/N ratio: it is very important both not to have a large noise before the amplification stage in order to not multiply that noise, and chose a reasonable threshold of the discriminator to cut noise-hits much as possible.

#### 2.4.1 Preamplifier

Even if circuits on the silicon crystal are only constructed by CMOS, a preamplifier can be modeled as an operational amplifier (OpAmp) where the gain is determined by the input and feedback impedance (first step in figure 2.7):

$$G = \frac{v_{out}}{v_{in}} = \frac{Z_f}{Z_{in}} \quad (2.8)$$

Depending on whether a capacity or a resistance is used as feedback, respectively a charge or a voltage amplifier is used: if the voltage input signal is large enough and have a sharp rise time, the voltage sensitive preamplifier is preferred. Consequently, this flavor doesn't suit to large fill factor MAPS whose signal is already enough high:  $v_{in} = Q/C_D \approx 3fC/100 \text{ pF} = 0.03 \text{ mV}$ , but it's fine for the small fill factor ones:  $v_{in} = Q/C_D \approx 3fC/3 \text{ pF} = 1 \text{ mV}$ .

In the case of a resistor feedback, if the signal duration time is longer than the discharge time ( $\tau = R_S C_D$ ) of the detector the system works as current amplifier, as the signal is immediately transmit to the amplifier; in the complementary case (signal duration longer than the discharge time) the system integrates the current on the  $C_D$  and operates as a voltage amplifier.

## 2.5 Readout logic

Readout logic includes the part of the circuit which takes the FE output signal, processes it and then transmit it out of pixel and/or out of chip; depending on the situation of usage different readout characteristics must be provided.

To store the analogical information (i.e. charge collected, evolution of signal in time, ...) big buffers and a large bandwidth are needed; the problem that doesn't occur, or better occur only with really high rate, if one wants record only digital data (if one pixel is hit 1 is recorded, and if not 0 is recorded).

A common compromise often made is to save the time over threshold (ToT) of the pulse in clock cycle counts; this needs of relatively coarse requirement as ToT could be trimmer to be a dozen bits but, being correlated and hopefully being linear with the deposited charge by the impinging particle in the detector, it provides a sufficient information. The ToT digitalization usually takes advantage of the distribution of a clock (namely BCID, bunch crossing identification) on the pixels' matrix. The required timing precision is at least around 25 ns, that corresponds to the period of bunch collisions at LHC; for such reason a reasonable BCID-clock frequency for pixels detector is 40 MHz.

Leading and trailing edges' timestamp of the pulse are saved on pixel within a RAM until they have been read, and then the ToT is obtained from their difference.

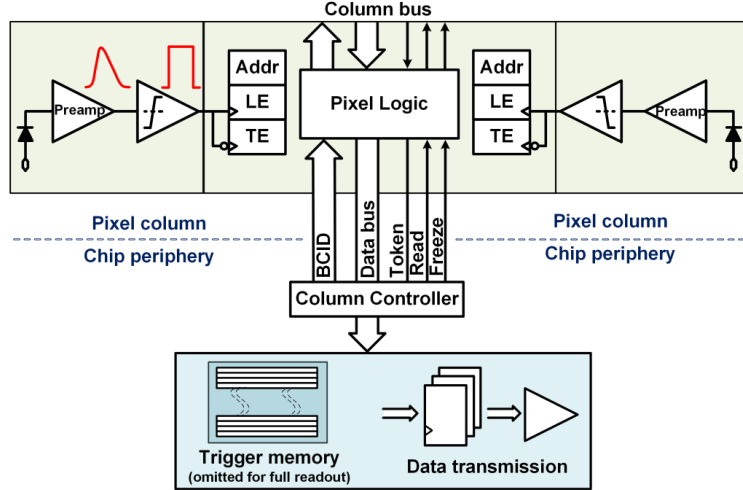


Figure 2.8: Column drain R/O scheme where ToT is saved

Moreover, the readout architecture can be full, if every hit is read, or triggered, if a trigger system decides if the hit must be stored or not. On one hand the triggered-readout needs buffers and storage memories, on the other the full readout, because there is no need to store hit data on chip, needs an high enough bandwidth.

A triggered readout is fundamental in accelerator experiments where the quantity of data to store is too large to be handled, and some selections have to be applied by the trigger: to give an order of growth, at LHC more than 100 TBit/s of data are produced, but the storage limit is about 100 MBit/s [3] (pag. 797).

Typically the trigger signal is processed in a few  $\mu s$ , so the pixel gets it only after a hundred clock cycles from the hit arrival time: the buffer depth must then handle the higher trigger latency.

After having taken out the data from the pixel, it has to be transmitted to the end of column (EoC) where a serializer delivers it out of chip, typically to an FPGA.

There are several ways of transmitting data from pixel to the end of column: one of the most famous is the column-drain read out, developed for CMS and ATLAS experiments [4]. All the pixels in a double-column share a data bus and only one pixel at a time, according to a priority chain, can be read. The reading order circuit is implemented by shift register (SR): when a hit arrives, the corresponding data, which can be made of timestamp and ToT, is temporarily stored on a RAM until the SR does not allow the access to memory by data bus.

Even if many readout architectures are based on the column-drain one, it doesn't suit for large size matrices. The problem is that increasing the pixels on a column would also raise the number of pixels in the priority chain and that would result in a slowdown of the readout.

If there isn't any storage memory, the double-column behaves as a single server queue and the probability for a pixel of waiting a time  $T$  greater than  $t$ , with an input hit rate on the column  $\mu$  and an output bandwidth  $B_W$  is [5]:

$$P(T > t) = \frac{\mu}{B_W} e^{-(B_W - \mu)t} \quad (2.9)$$

To avoid hit loss (let's neglect the contribution to the inefficiency of the dead time  $\tau$  due to the AFE), for example imposing  $P(T > t) \sim 0.001$ , one obtains  $(B_W - \mu) t_t \sim 6$ , where  $t_t$  is the time needed to transfer the hit; since  $t_t$  is small, one must have  $B_W \gg \mu$ , that means a high bandwidth [5].

Actually the previous one is an approximation since each pixel sees a different bandwidth depending on the position on the queue: the first one sees a full bandwidth, but the next sees a smaller one because occasionally it can be blocked by the previous pixel. Then the bandwidth seen by the pixel  $i$  is  $B_i = B - \sum_j \mu_j$ , where  $\mu_j$  is the hit rate of the  $j$ th pixel.

The efficiency requirement on the bandwidth and the hit rate becomes:  $B_{W,i} > \mu_i$ , where the index  $i$  means the constraint is for a single pixel; if all the  $N$  pixels on a column have the same rate  $\mu = N\mu_i$ , the condition reduces to  $B_W > \mu$ . The bandwidth must be chosen such that the mean time between hits of the last pixel in the readout chain is bigger than that.

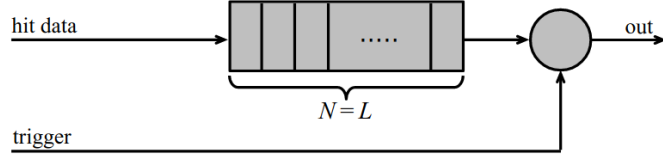


Figure 2.9: Block diagram of a pipeline buffer:  $N$  is the dimension of memory buffer and  $L$  is the trigger latency expressed in BCID cycles

264 In order to reduce the bandwidth a readout with zero suppression on pixel is typically employed;  
 265 this means that only information from channels where the signal exceeds the discriminator thresh-  
 266 old are stored. Qu'è succiso con la zero suppression? La metto qui questa affermazione?

267 If instead there is a local storage until a trigger signal arrives, the input rate to column bus  
 268  $\mu'$  is reduced compared to the hit rate  $\mu$  as:  $\mu' = \mu \times r \times t$ , where  $r$  is the trigger rate and  $t$  is  
 269 the bunch crossing period. In this situation there is a more relaxed constraint on the bandwidth,  
 270 but the limiting factor is the buffer depth: the amount of memory designed depends both on the  
 271 expected rate  $\mu$  and on the trigger latency  $t$  as  $\propto \mu \times t$ , that means that the higher the trigger  
 272 latency and the lower the hit rate to cope with.

273 In order to have an efficient usage of memory on pixels' area it's convenient grouping pixels  
 274 into regions with shared storage. Let's compare two different situations: in the first one a buffer  
 275 is located on each pixel area, while in the second one a core of four pixels share a common buffer  
 276 (this architecture is commonly called FE-I4).

Consider a 50 kHz single pixel hits rate and a trigger latency of 5  $\mu s$ , the probability of losing

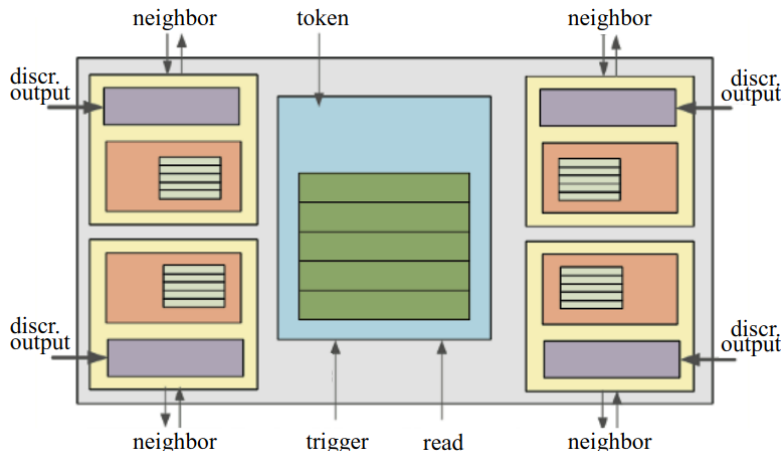


Figure 2.10: Block diagram of the FE-I4 R/O. Read and memory management section is high-  
 lighted in light blue; latency counters and trigger management section are highlighted in green;  
 hit processing blocks are highlighted in purple; ToT counters and ToT management units are  
 highlighted in orange

277 hits is:  
 278

$$P(N > 1|\nu) = 1 - P(N = 0|\nu) - P(N = 1|\nu) = 1 - e^{-\nu}(1 + \nu) \approx 2.6\% \quad (2.10)$$

279 where I have assumed a Poissonian distribution with mean  $\nu = 0.25$  to describe the counts  $N$ .  
 280 To get an efficiency  $\epsilon$  greater than 99.9 % a 3 hit depth buffer is needed:

$$P(N > 3|\nu) = 1 - \sum_{i=0}^3 P(N = i|\nu) < 0.1\% \quad (2.11)$$

281 Considering the second situation: if the average single pixel rate is still 50 kHz, grouping four  
 282 pixels the mean number of hits per trigger latency is  $\nu = 0.25 \times 4 = 1$ . To get an efficiency of  
 283 99.9% (eq. 2.11) a buffer depth of 5 hits in the four-pixels region, instead of 3 per pixels, is needed.

<sup>284</sup> **Chapter 3**

<sup>285</sup> **Use of pixels detector**

<sup>286</sup> A partire dal 2017, i sensori CMOS rappresentano l'89% delle vendite globali di sensori di immagine.  
<sup>287</sup> Ma praticamente dal 2010 in poi solo CMOS e non più CCD.

<sup>288</sup>

<sup>289</sup> **3.1 Tracking in HEP**

<sup>290</sup> Per gli acceleratori la richieste sono molto stringenti e lo saranno sempre di più con l'aumento dell'  
<sup>291</sup> intensità o della luminosità in termini di radiation hardness (per HL-LHC for example expected  
<sup>292</sup> in 5 anni 500 Mrad e NIEL di 10 alla 16), efficiency e occupancy (efficienza alta dopo tanta  
<sup>293</sup> radiazione e noise occupancy bassa), time resolution (bunch crossing 40 Mhz), material budget e  
<sup>294</sup> power consumption (material budget below 2 per cento e power consumption 500 mW/cm<sup>2</sup>)  
<sup>295</sup> Usati come tracciatori per misure di impulso e per misure di energia (per rigettare ) ad esempio  
<sup>296</sup> dati di fondo (topic fondamentale per BELLE-II).

<sup>297</sup> **Resolution**

<sup>298</sup> Depending on the type of signal reading the spatial resolution is  $\sigma_x = \frac{p}{\sqrt{12}}$  where p is the pitch  
<sup>299</sup> between pixels, or even better if other analogica information, as the charge, are read and capacitive  
<sup>300</sup> charge division method is applied.

<sup>301</sup> **3.1.1 Hybrid pixels: ATLAS, CMS and LHC-b**

<sup>302</sup> **3.1.2 CMOS MAPS: ALICE and STAR**

<sup>303</sup> I've already mentioned ALICE pixel dector talking about the new process modification, now the  
<sup>304</sup> ALICE name comes up again talking about FE: this is because ALPIDE (ALice PIxel DEtector)  
<sup>305</sup> is one of the first MAPS detector (TowerJazz 180 nm CMOS) installed <sup>1</sup>, therefore it is the current  
<sup>306</sup> state-of-art and most of the following chips' FE are inspired by that, making it a standard in the  
<sup>307</sup> FE design.

<sup>308</sup> For years ALICE have been pioneering MAPS detectors and its sensors are currently state-of-  
<sup>309</sup> the art in this sector, to the point that most of today's CMOS MAPS chips implement the same  
<sup>310</sup> FE of ALICE Pixel Detector, and in fact they are commonly called "ALPIDE-like" sensors<sup>2</sup>.

<sup>311</sup> **3.2 Application in medical imaging**

<sup>312</sup> **3.2.1 Medipix and Timepix**

<sup>313</sup> **3.2.2 Applicability to FLASH radiotherapy**

---

<sup>1</sup>It was installed in the Inner Tracking System during the second long shut down of the LHC in 2019

<sup>2</sup>As we'll see TJ-Monopix1 and ARCADIA have an ALPIDE-like front end.

<sup>314</sup> **Chapter 4**

<sup>315</sup> **TJ-Monopix1**

<sup>316</sup>

- <sup>317</sup> • scrivere la differenza tra i FE
- <sup>318</sup> • fare disegno uguale a quello del mascheramento però con solo due coordinate
- <sup>319</sup> • scrivere delle misure cambiando i parametri del FE, e rifare le misure del FE con oscilloscopio e qualche plot
- <sup>320</sup> • scrivere misure del tempo morto e rifarle

<sup>322</sup> The TJ-Monopix1 is one of the chips fabricated by TowerJazz with 180 CMOS imaging process.  
<sup>323</sup> From the middle of 2013 a dedicated collaboration, RD 53 ('Development of pixel readout integrated  
<sup>324</sup> circuits for extreme rate and radiation'), has been established with the specific goal to find  
<sup>325</sup> a sensor suitable as vertex detector for future upgrade of CMS and ATLAS experiments. Among  
<sup>326</sup> the main objects of study of the collaboration there are both hybrid pixels and monolithic options  
<sup>327</sup> as CMOS MAPS: fig 4.1 shows the intermediate MAPS-prototypes made by TowerJazz.

Besides the TowerJazz series, also LFoundry fabricated other similar sensors with 150 CMOS

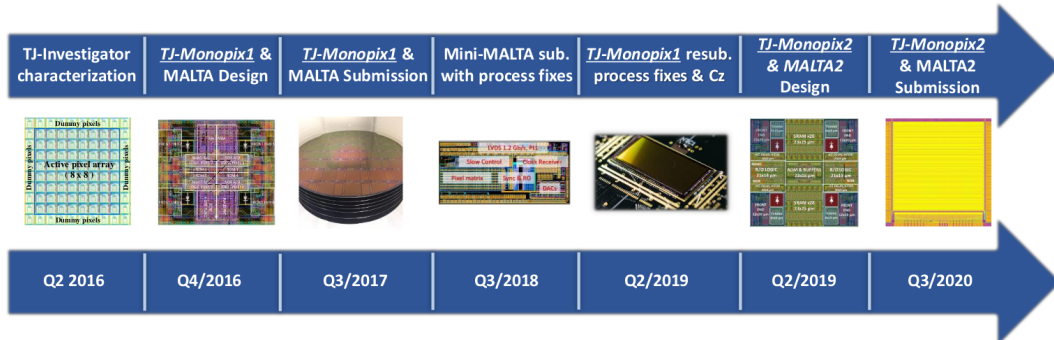


Figure 4.1: Timeline in TowerJazz productions. In addition to Monopix series also the small electrode demonstrator TJ-Malta and mini-Malta have been produced and tested[6]. The Malta prototypes differ from TJ-Monopix in the readout: while Monopix implements a column-drain R/O, an asynchronous R/O without any distribution of BCID has been used by TJ-Malta in order to reduce power consumption.

<sup>328</sup>  
<sup>329</sup> technology [7][8]: LF-Monopix.  
<sup>330</sup> The main differences between the LFoundry and TowerJazz's products (tab. 4.2), are in the sensor  
<sup>331</sup> structure rather than in the readout architecture, based on a column drain R/O with ToT capability  
<sup>332</sup> (LF-Monopix has 8 bits dedicated and TJ-Monopix 6 bits). Concerning the sensor, LFoundry  
<sup>333</sup> pixels are bigger and have a large fill factor, while TJ-Monopix ones have a small fill-factor elec-  
<sup>334</sup> trode.

<sup>335</sup> The performances of both the detectors have been tested before and after irradiation ( $\sim 10^{10} n_{eq}/cm^2$ ) and the result is, as expected since LF-Monopix is a large fill factor electrode (chap.  
<sup>336</sup> ??), that LF-Monopix is more radiation hard than TJ-Monopix whereas the main degradation of

|                    | LF-Monopix1   | TJ-Monopix1   |
|--------------------|---|---|
| Bulk Resistivity   | p-type substrate<br><i>maggior</i> $2\text{k}\Omega\text{cm}$ | p-epi. on a low $\rho$ substrate<br><i>maggior</i> $1\text{k}\Omega\text{cm}$ |
| Pixel size         | $50 \times 250 \mu\text{m}^2$                                 | $26 \times 40 \mu\text{m}^2$  |
| Depth              | $100\text{-}750 \mu\text{m}$                                  | $25 \mu\text{m}$  |
| Capacity           | $\sim 400 \text{ fF}$   | $\sim 3 \text{ fF}$   |
| Preamplifier       | CSA   | Voltage   |
| Threshold trimming | on pixel (4-bit DAC)  | global threshold  |
| Readout mode       | Fast column drain   | Fast column drain   |
| Consumption        | $\sim 300 \text{ mW/cm}^2$                                    | $\sim 120 \text{ mW/cm}^2$  |
| Threshold          | $1500 e^-$  | $\sim 270 e^-$  |
| ENC                | $100 e^-$   | $\sim 30 e^-$   |

Table 4.1: Main characteristics of TJ-Monopix and LF-Monopix [8]

| Parameter         | Value                        |
|-------------------|------------------------------|
| Matrix size       |                              |
| Pixel size        | $26 \times 40 \mu\text{m}^2$ |
| Depth             | $25 \mu\text{m}$             |
| BCID              | 40 MHz                       |
| ToT-bit           | 6                            |
| Power consumption | $\sim 120 \text{ mW/cm}^2$   |

Table 4.2

efficiency in TJ-Monopix chips is due to the low electric field in the pixel corner. On the other hand one more accidental consequence of the large fill factor size in LF-Monopix (the deep p-well covers  $\sim 55 \%$  of the pixel area) is a significant cross-talk problem.

## 4.1 The sensor

TJ-Monopix1 adopts the modification described in ?? that allows to achieve a planar depletion region near the electrode applying a relatively small reverse bias voltage: a low dose n implant is build on a high resistivity ( $\geq 1 \text{ k}\Omega \text{ cm}$ ), p-type epitaxial layer.

This modification improves the efficiency of the detector, especially after irradiation[]; however a Technology Computer Aided Design (TCAD) simulation has shown that a nonuniform electric field is still produced in the lateral regions after the modification; since the transversal component of the electric field drops at the pixel corner (this point in figure 4.2 is indicated by a star) the efficiency at the side is reduced.

On a sample of chip, the one I've tested in Pisa belongs to these, a second optimization have been made to enhance the lateral component of electric field and improve the efficiency and velocity in charge collection near the corners of the sensor: a portion of low dose implant has been removed, creating a step discontinuity in the pixel corner. A side effect is the weaker separation between the deep p-well and the p-substrate, that cannot be biased separately anymore to prevent the punchthrough. Moreover, to investigate the charge collection properties, as the threshold, the noise and the efficiency, pixels within the matrix feature a difference in the doping structure of the deep p-well: rows from 0 to 111 are fully covered by deep p-well (FDPW) under p-well near the sensor, while rows from 112 till the last 223 have a portion of deep p-well removed (RDPW). The removing enhance the lateral electric field component then resulting in a higher efficiency, as we'll see later.

361

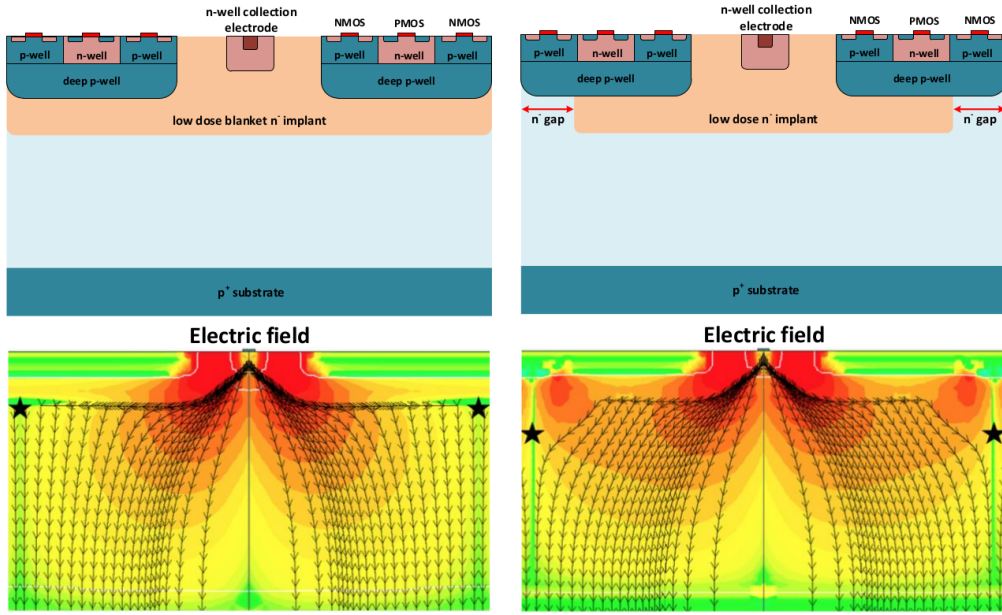


Figure 4.2: (a) The cross-section of a monolithic pixel in the TJ-Monopix 180 nm with modified process; additionally in (b) a gap in the low dose implant is created to improve the collection of charge due to a bigger lateral component of the electric field

## 4.2 FE flavors

TJ-Monopix1 has been implemented in four different flavors, each one corresponding to a different sector on the matrix (fig. 4.3) and thus having a separate readout and data transmission, in order to explore different variations of the FE. The four flavors mainly differ in the reset input circuit. R resistenza di reset deve essere abbastanza grande in modo da far sì che il ritorno allo

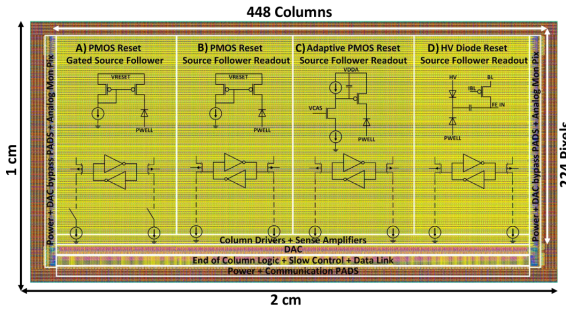


Figure 4.3

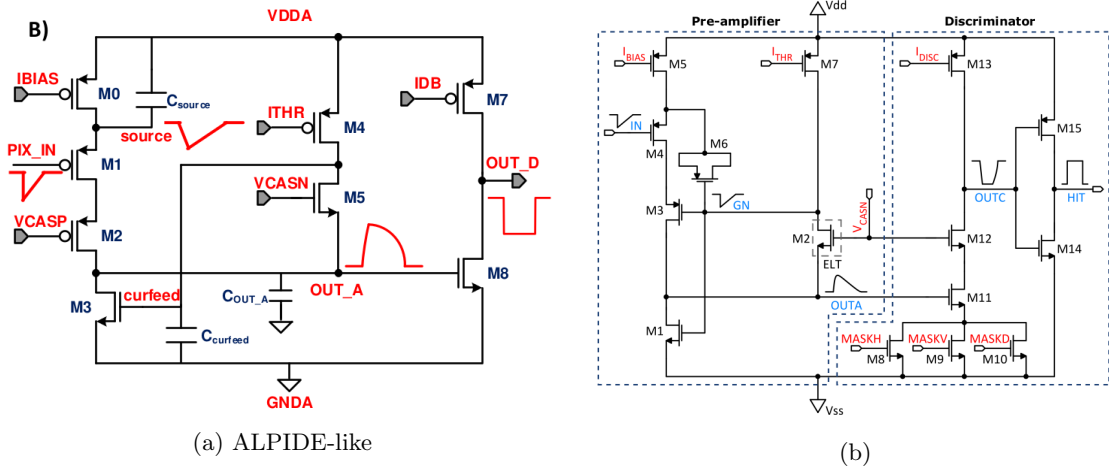
zero è abbastanza lento (non devi "interferire" con la tot slope e non devi più corto del tempo del preamplificatore, sennò hai perdita di segnale).  
Baseline reset: all'input solitamente hai un PMOSS o un diodo;

### 4.2.1 ALPIDE-like front end

As I already mentioned, ALICE Pixel Detector (ALPIDE) is the current state-of-art and most of the following chips' FE are inspired by that, making it a standard in the FE design

The idea of the amplification stage is to transfer the charge from a bigger capacity[2],  $C_{source}$ , to a smaller one,  $C_{out}$ : the input transistor M1 with current source IBIAS acts as a source follower and this forces the source of M1 to be equal to the gate input  $\Delta V_{PIX\_IN} = Q_{IN}/C_{IN}$ .

$$Q_{source} = C_{source} \Delta V_{PIX\_IN} \quad (4.1)$$



376 The current in M2 and the charge accumulates on  $C_{out}$  is fixed by the one on  $C_{source}$ :

$$\Delta V_{OUT\_A} = \frac{Q_{source}}{C_{OUT\_A}} = \frac{C_{source} \Delta V_{PIX\_IN}}{C_{OUT\_A}} = \frac{C_{Source}}{C_{OUT\_A}} \frac{Q_{IN}}{C_{IN}} \quad (4.2)$$

377 A second branch (M4, M5) is used to generate a low frequency feedback, where VCASN and ITHR  
378 set the baseline value of the signal on  $C_{OUT\_A}$  and the velocity to goes down to the baseline.

379 **IL RUOLO DI CURVFEED NON L'HO CAPITO.**

380 Finally IDB defines the charge threshold with which the signal  $OUT\_A$  must be compared: depending on if the signal is higher than the threshold or not, the  $OUT\_D$  is high or low respectively.

382 The FE circuit 4.4b is ALPIDE-like, so it is similar to the one described in ??; a quanto già  
383 detto voglio però aggiungere due parole: come viene implementato il mascheramento dei pixels e  
384 il reset.

385

386 In order to reduce the hit rate and to avoid saturating the bandwidth, is uttermost important  
387 to include in the FE a way to mask noisy pixels, which typically are those with manufacturing  
388 defects. In the circuit in fig. 4.4b transistors M8, M9 and M10 have the function of disabling  
389 registers with coordinates MASKH, MASKV and MASKD (respectively vertical, orizontal and  
390 diagonal) from readout: if all three transistors-signals are low, the pixel's discriminator is disabled.  
391 Compared with a configurable masking register which would allow disableing pixels individually,  
392 to use a triple redundancy reduces the sensistivity to SEU<sup>1</sup> but also gives amount of intentionally  
393 masked ("ghost") pixels. This approach is suitable only for extremely small number N of pixel has  
394 to be masked: if two coordinate projection scheme had been implemented, the number of ghost  
395 pixels would have scale with  $N^2$ , if instead three coordinates are used, the N's exponential is lower  
396 than 2 (fig. 4.5)

#### 397 4.2.2 FE parameters

398 Descrivo un po' le misure fatte sul fe e sul significato dei vari parametri.  
399 it allows injecting pixels with a known charge in DAC units.

### 400 4.3 Readout logic

401 TJ-Monopix1 has a triggerless, fast and with ToT capability R/O which is based on a column-drain  
402 architecture. On the pixel are located two Random Access Memory (RAM) cells to store the 6-bit  
403 LE and 6-bit TE of the pulse, and a Read-Only Memory (ROM) containing the 9-bit pixel address.

<sup>1</sup>Single Event Upset, in sostanza è quando un bit ti cambia valore (da 0 a 1 o viceversa) perché una particella deposita carica nell'elettronica che fa da memoria registro/RAM/.... Questo tipo di elettronica ha bisogno di un sacco di carica prima che il bit si "flippi" (cambi valore), infatti tipicamente per avere un SEU non basta una MIP che attraversa esattamente quel pezzo di chip in cui è implementata la memoria, ma un adrone che faccia interazione nucleare producendo più carica di quanto farebbe una MIP. Questo metodo pur essendo più comodo richiede less amount of area ha però come drawback che il registro può essere soggetto a SEU problema non trascurabile in acceleratori come HL-LHC adronici

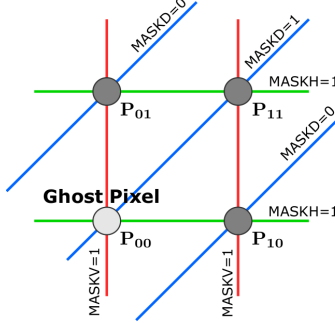


Figure 4.5

| Parameter | Meaning |
|-----------|---------|
| IBIAS     |         |
| IDB       |         |
| ITHR      |         |
| VCASN     |         |
| VREF      |         |
| IREF      |         |

Table 4.3

404 Excluded these memories, TJ-Monopix1 hasn't any other buffer: if a hit arrives while the pixel is  
 405 already storing a previous one, the new data get lost. After being read, the data packet is sent to  
 406 the EoC periphery of the matrix, where a serializer transfers it off-chip to an FPGA (4.6). There  
 407 a FIFO is used to temporarily stored the data, which is transmitted to a computer through an  
 408 ethernet cable in a later time.

409 The access to the pixels' memory and the transmission of the data to the EoC is based on  
 410 a Finite State Machine (FSM) composed by four state: no-operation (NOP), freeze (FRZ), read  
 411 (RD) and data transfer (DTA). The readout sequence (4.7) starts with the TE of a pulse: the  
 412 pixel immediately tries to grab the column-bus turning up a hit flag signal called *token*. The token  
 413 is used to control the priority chain and propagates across the column indicating what pixel that  
 414 must be read. To start the readout and avoid that the arrival of new hits disrupt the priority logic,  
 415 a *freeze* signal is activated, and then a *read* signal controls the readout and the access to memory.  
 416 During the freeze, the state of the token for all pixels on the matrix remains settled: this does  
 417 not forbid new hits on other pixels from being recorded, but forbids pixels hit from turning on the  
 418 token until the freeze is ended. The freeze stays on until the token covers the whole priority chain  
 419 and gets the EoC: during that time new token cannot be turned on, and all hits arrived during  
 420 a freeze will turn on their token at the end of the previous freeze. Since the start of the token is  
 421 used to assign a timestamp to the hit, the token time has a direct impact on the time resolution  
 422 measurement; this could be a problem coping with high hits rate.

423 The analog FE circuit and the pixel control logic are connected by an edge detector which is  
 424 used to determine the LE and the TE of the hit pulse(fig. 4.8): when the TE is stored in the first  
 425 latch the edge detector is disabled and, if the **FREEZE** signal is not set yet, the readout starts. At  
 426 this point the HIT flag is set in a second latch and a token signal is produced and depending on  
 427 the value of **Token** in the pixel can be read or must wait until the **Token in** is off. In figure an OR  
 428 is used to manage the token propagation, but since a native OR logic port cannot be implemented  
 429 with CMOS logic, a sum of a NOR and of an inverter is actually used; this construct significantly  
 430 increases the propagation delay (the timing dispersion along a column of 0.1-0.2 ns) of the token  
 431 and to speed up the circuit optimized solution are often implemented. When the pixel become the  
 432 next to be read in the queue, and at the rising edge of the **READ** signal, the state of the pixel is  
 433 stored in a D-latch and the pixel is allowed to use the data bus; the TE and the HIT flag latches  
 434 are reset and a **READINT** signal that enable access of the RAM and ROM cells is produced.

435  
 436 The final data must provide all the hits' information: the pixel address, the ToT and the

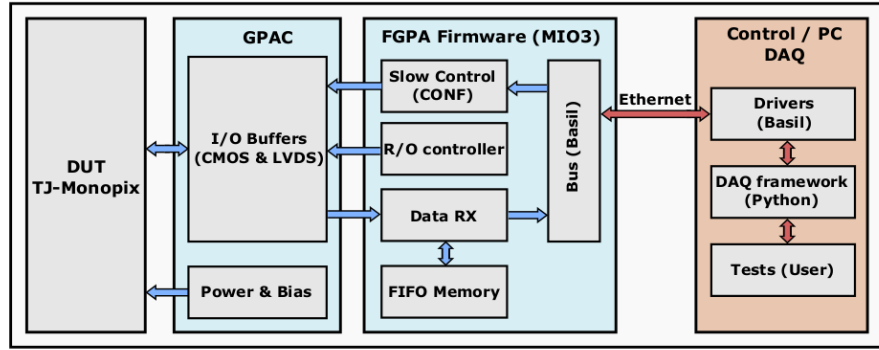
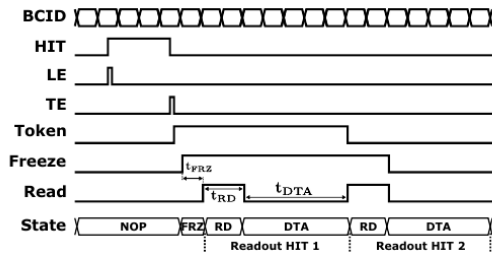


Figure 4.6: Main caption



(b) Readout sequence timing diagram. In this example two hits are being processed.

Figure 4.7: Readout timing diagram: in this example two hits are being processed

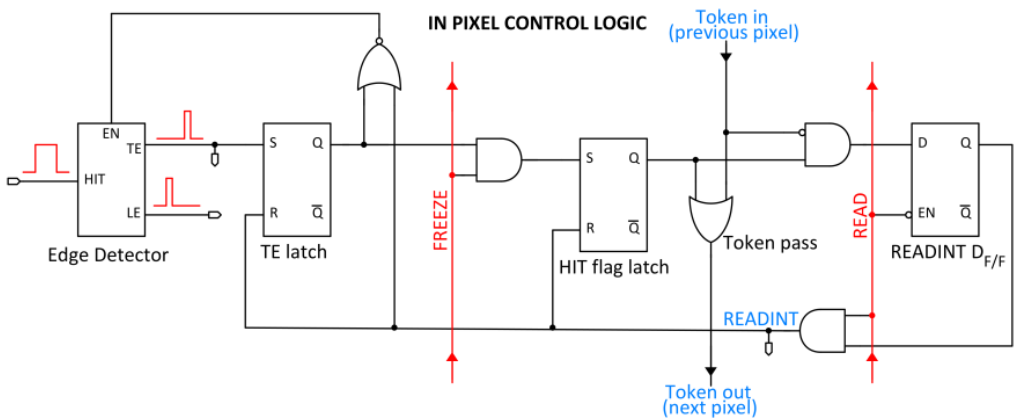


Figure 4.8

437 timestamp. All those parts are assigned and appended at different time during the R/O chain:

- 438 • **Pixel address:** while the double column address (6-bit) is appended by the EoC circuit,  
439 the row address (8-bits for each flavor) and the physical column in the doublet (1-bit) are  
440 assigned by the in-pixel logic
- 441 • **ToT:** is obtained offline from the difference of 6-bits TE and 6-bits LE, stored by the edge  
442 detector in-pixel; since a 40 MHz BCID is distributed across the matrix, the ToT value is  
443 range 0-64 clock cycle which corresponds to 0-1.6  $\mu$ s
- 444 • **Timestamp:** The timestamp of the hit correspond to the time when the pixel set up the  
445 token; it is assigned by the FPGA, that uses the LE, TE and a 640 MHz clock to derive it

446 When the bits are joined up together the complete hit data packet is 27-bit.

#### 447 4.3.1 Dead time measurement

448 Only one hit at a time can be stored on the pixel's RAM, so until the data have completed the  
449 path to get out, the pixel readout is paralyzed; so, the dead time corresponds with the time needed  
450 to export the data-packets. To measure that quantity, that is a function of the hit rate I've used  
451 the injection circuit available on matrix that allows fixing not only the amplitude (charge in DAC)  
452 of the pulse but also the period and width. Reducing the distance between two consecutive pulses  
453 and finding the value when the efficiency decrease, one can estimates the dead time. Dal momento  
454 che c'è un solo serializzatore e che quindi la lettura è sequenziale per tutto il flavor e per quanto  
455 detto sul funzionamento del R/O, il  $\tau$  dipende in maniera lineare dal numero di pixel contenenti  
456 una hit. Per verificare l'andamento lineare e valutare quanto fosse il tempo morto in funzione del  
457 rate ho effettuato uno scan nel rate (diminuendo il periodo tra gli impulsi) e nel numero di pixel  
458 iniettati.

459 Il collo di bottiglia del tempo morto è dato dal fatto che c'è un unico serializzatore, infatti per  
460 trasmettere i dati dal pixel alla EoC è necessario un solo ciclo di clock dal momento che c'è un  
461 data bus da n-bit. Per definire meglio il  $\tau$  faccio riferimento alla fig ??: se una hit arriva su un  
462 pixel mentre ha il token alto allora la hit viene persa. Se una hit arriva su un pixel che non ha il  
463 token alto ma ha il freeze alto, allora non viene persa ma le viene assegnato un timestamp errato.

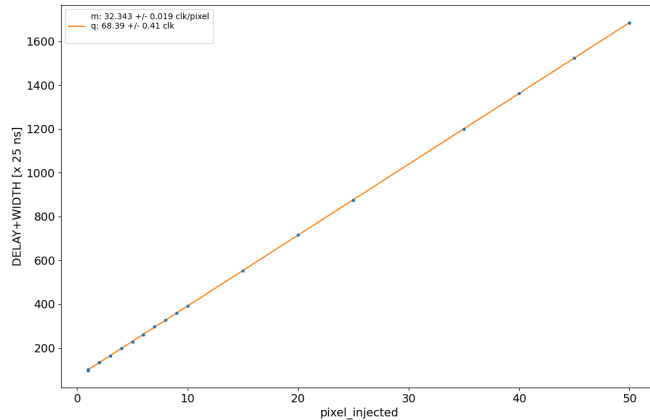


Figure 4.9

464 A tutte le hit di una iniezione che arrivano contemporaneamente viene assegnato lo stesso  
465 timestamp; quando le hit iniziano ad essere meno di quelle che mi aspetti. Mappa in funzione delle  
466 iniezioni di quali pixel hai letto.

# 467 Chapter 5

## 468 Arcadia-MD1

469 [9] [10]

470 Breve introduzione analoga a Monopix1 in cui descrivo brevemente la "timeline" da SEED  
471 Matisse a Md1 e Md2

### 472 5.1 The sensor

473 ARCADIA-MD1 is an LFoundry chip which implements the technology 110 nm CMOSS node  
474 with six metal layer ???. The standard p-type substrate was replaced with an n-type floating zone  
475 material, that is a tecnique to produce purified silicon crystal. (pag 299 K.W.).

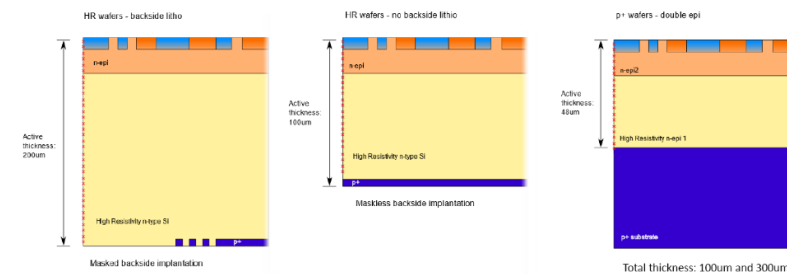


Figure 5.1

476  
477 Wafer thinning and backside litography were necessary to introduce a junction at the bottom  
478 surface, used to bias the substrate to full depletion while maintaining a low voltage at the front side.  
479 C'è un deep pwell per - priority chainseparare l'elettronica dal sensore; per controllare il punchthrough  
480 è stato aggiunto un n doped epitaxial layer having a resistivity lower than the substrate.

481 RILEGGI SUL KOLANOSKY COS'È IL PUNCHTHROUGHT, FLOAT ZONE MATERIAL,  
482 COME VENGONO FATTI I MAPS COME FAI LE GIUNZIONI

483 It is part of the cathegory of DMAPS Small electrode to enhance the signal to noise ratio.  
484 It is operated in full depletion with fast charge collection by drift.

485 Prima SEED si occupa di studiare le prestazioni: oncept study with small-scale test struc-  
486 ture (SEED), dopo arcadia: technology demonstration with large area sensors Small scale demo  
487 SEED(sensor with embedded electronic developement) Quanto spazio dato all'elettronica sopra il  
488 pwell e quanto al diodo. ..

### 489 5.2 Readout logic and data structure

#### 490 5.2.1 Matrix division and data-packets

491 The matrix is divided into an internal physical and logical hierarchy: The 512 columns are divided  
492 in 16 section: each section has different voltage-bias + serializzatori. Each section is devided in

493 cores () in modo che in ogni doppia colonna ci siano 1Pacchetto dei dati 6 cores. ricordati dei serializzatori: sono 16 ma possono essere ridotti ad uno in modalità spazio

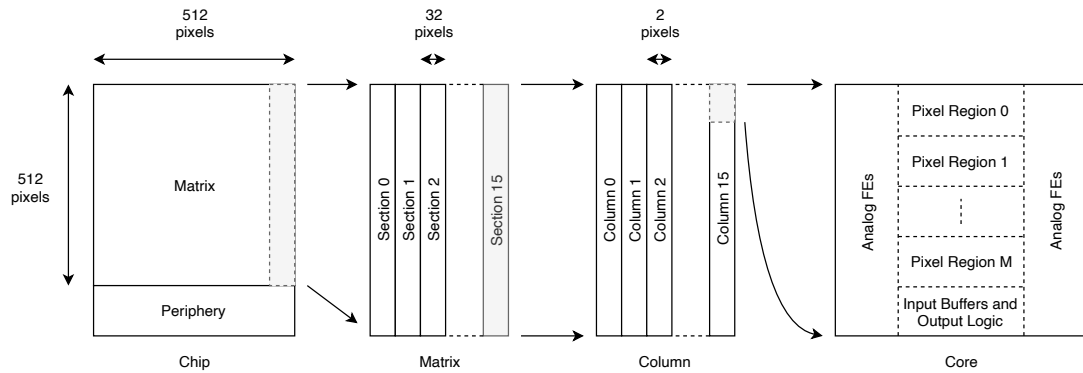


Figure 5.2

494

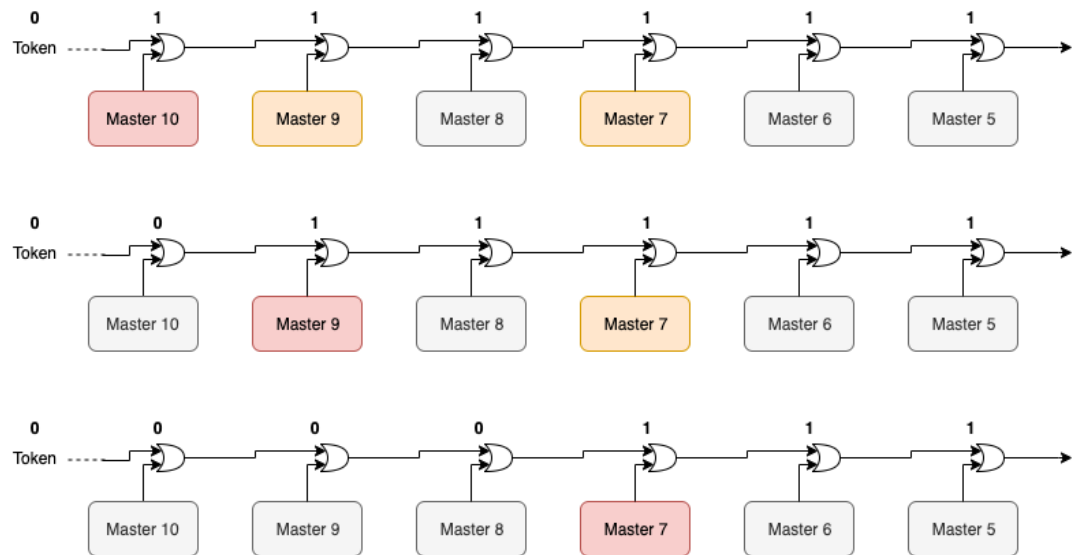


Figure 5.3

495 Questa divisione si rispecchia in come sono fatti i dati: scrivi da quanti bit un dato è fatto e le varie coordinate che ci si trovano dentro; devi dire che c'è un pixel hot e spieghi dopo a cosa serve, e devi accennare al timestamp  
496  
497

498 "A core is simply the smallest stepped and repeated instance of digital circuitry. A relatively  
499 large core allows one to take full advantage of digital synthesis tools to implement complex func-  
500 tionality in the pixel matrix, sharing resources among many pixels as needed.". pagina 28 della  
501 review.

502

503 TABELLA: con la gerarchia del chip Matrix (512x512 pixels) Section (512x32 pixels) Column  
504 (512x2) Core (32x2) Region (4x2)

505 Nel chip trovi diverse padframe: cosa c'è nelle padframe e End of section.

506 "DC-balance avoids low frequencies by guaranteeing at least one transition every n bits; for  
507 example 8b10b encoding n =5"

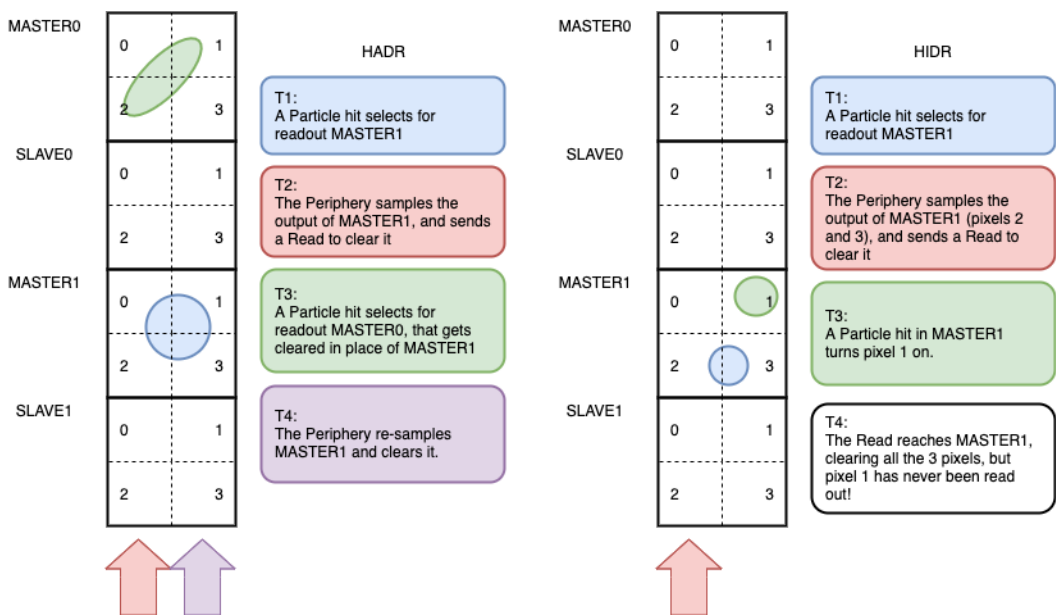


Figure 5.4

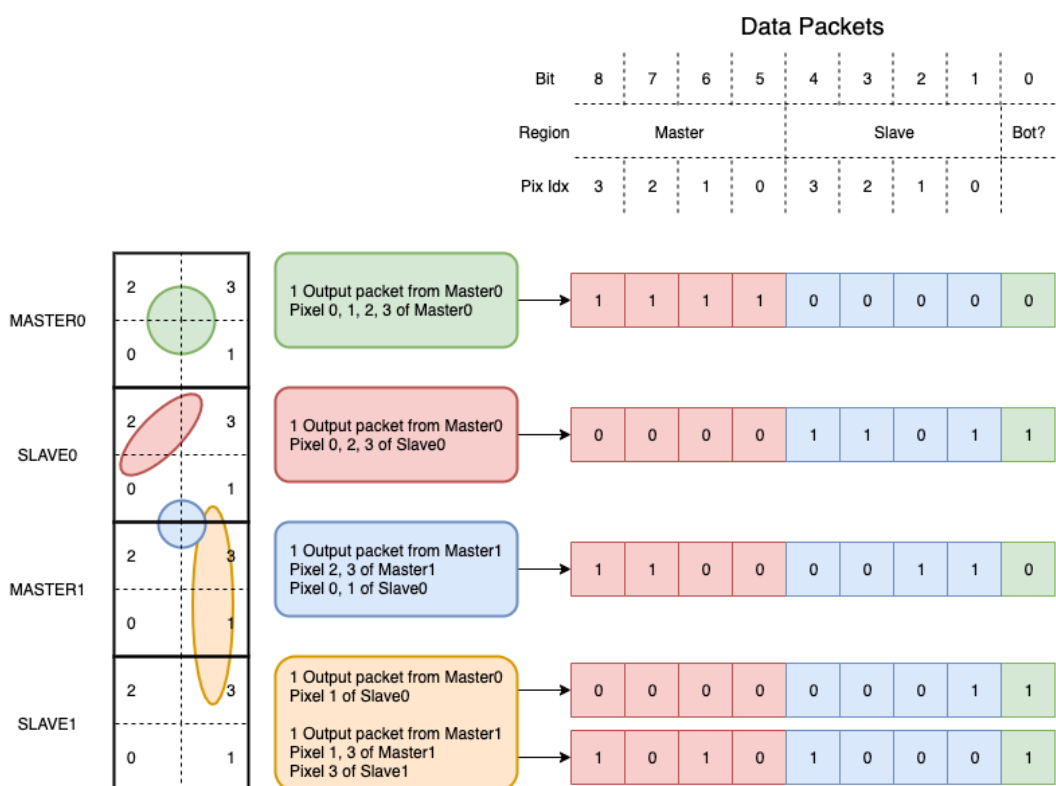


Figure 5.5

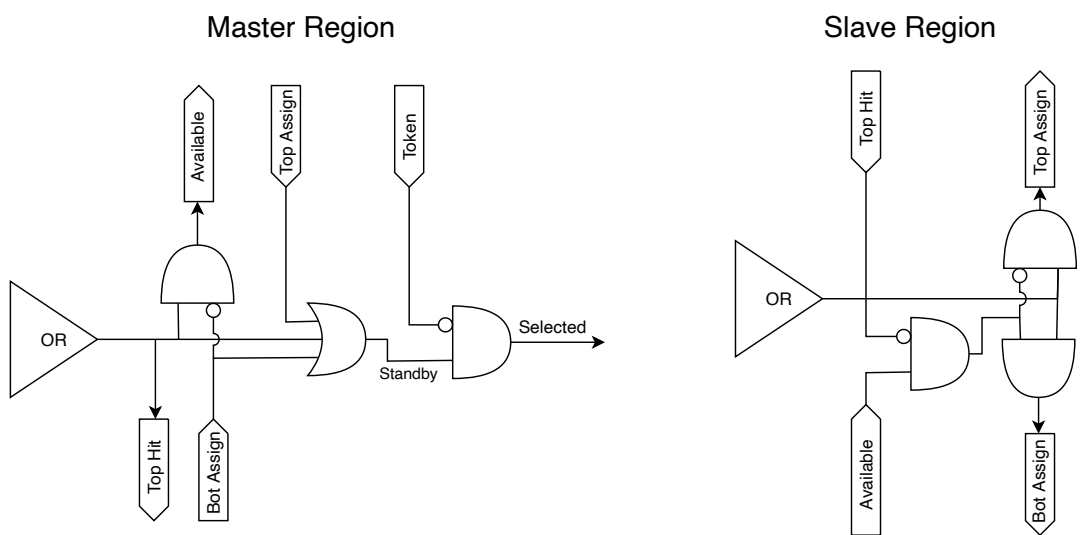


Figure 5.6

508    **Chapter 6**

509    **Threshold and noise  
510    characterization**

511    **6.1 Threshold and noise: figure of merit for pixel detectors**

512    The signal to threshold ratio is the figure of merit for pixel detectors.

513  
514    la soglia deve essere abb alta da tagliare il rumore ma abb bassa da non perdere efficienza.  
515    Invece di prendere il rapporto segnale rumore prendi il rapporto segnale soglia. Perchè? la soglia  
516    è collegato al rumore, nel senso che: supponiamo di volere un occupancy di 10-4 allora sceglierò la  
517    soglia in base a questo. (plot su quaderno) Da questo conto trovo la minima soglia mettibile  
518    In realtà quello che faccio è mettere una soglia un po' più grande perchè il rate di rumore dipende  
519    da molti fattori quali la temperatura, l annealing ecc, e non voglio che cambiando leggermente uno  
520    di questi parametri vedo alzarsi molto il rate di rumore. In realtà non è solo il rumore sensibile a  
521    diversi fattori, ma anche la soglia: ad esempio la cosa classica è la variabilità della soglia da pixel  
522    a pixel.

523    In questo modo rumore e soglia diventano parenti.

524    Review pag 26.

525    The noise requirement can be expressed as:

526    Questo implica tra le altre cose che voglio poter assegnare delle soglie diverse a diversi pixel:  
527    Drawback è dare spazio per registri e quantaltro.  
528    Questo lascia però ancora aperto il problema temporale delle variazioni del rumore: problema per  
529    cui diventano necessarie le misure dei sensori dopo l'irraggiamento.

530  
531    Per arcadia i registri (c'è un DAC) per la soglia (VCASN) si trovano in periferia. Non fare  
532    trimming sulla soglia è uno dei problemi che si sono sempre incontrati: a casusa dei mismatch dei  
533    transistor le soglie efficaci pixel per pixel cambiano tanto. La larghezza della s curve è il noise se se  
534    assumi che il noise è gaussiano

535    Il trimming della soglia avviene con dei DAC: la dispersione della soglia dopo al tuning e dovuta  
536    al dac è:

$$\sigma_{THR,tuned} = \frac{\sigma_{THR}}{2^{nbit}} \quad (6.1)$$

537    dove il numero di bit cambia varia tra 3-7 tipicamente. Monopix è 7 Arcadia 6

538  
539    Each ROIC is different in this respect, but in general the minimum stable threshold was around  
540    2500 electrons (e) in 1st generation ROICs, whereas it will be around 500 e for the 3rd generation.  
541    This reduction has been deliberate: required by decreasing input signal values. Large pixels (2 104  
542    um<sup>2</sup>), thick sensors (maggiore di 200 um), and moderate sensor radiation damage for 1st generation  
543    detectors translated into expected signals of order 10 ke, while small pixels (0.25 104 um<sup>2</sup>), thinner  
544    sensors (100 um), and heavier sensor radiation damage will lead to signals as low as 2 ke at the  
545    HL-LHC

546    The ENC can be directly calculated by the Cumulative Distribution Function (CDF) (scurve)  
547    obtained from the discriminator "hit" pulse response to multiple charge injections

## **548 6.2 TJ-Monopix1 characterization**

549 Com'è fatto il set up per le misure.  
550 FPGA BB, Chip con FE board, qualche foto  
551

## **552 6.3 ARCADIA-MD1 characterization**

553 Com'è fatto il set up per le misure.  
554 FPGA BB, Chip con FE board, qualche foto  
555

556 **Appendix A**

557 **Pixels detector: a brief overview**

558 **A.1 Radiation damages**

559 Radiation hardness is a fundamental requirement for pixels detector especially in HEP since they  
 560 are almost always installed near the interaction point where there is a high energy level of radiation.  
 561 At LHC the  $\phi_{eq}$  per year in the innermost pixel detector is  $10^{14} n_{eq}/cm^2$ ; this number reduces by  
 562 an order passing to the outer tracker layer [3] pag 341 Wermes. Here the high fluence of particles  
 563 can cause a damage both in the substrate of the detector and in the superficial electronics.

564 The first one has a principal non ionizing nature, due to a non ionizing energy loss (NIEL), but  
 565 it is related with the dislocation of the lattice caused by the collision with nuclei; by this fact the  
 566 NIEL hypothesis states that the substrate damage is normalized to the damage caused by 1 MeV  
 567 neutrons. Differently, surface damages are principally due to ionizing energy loss.

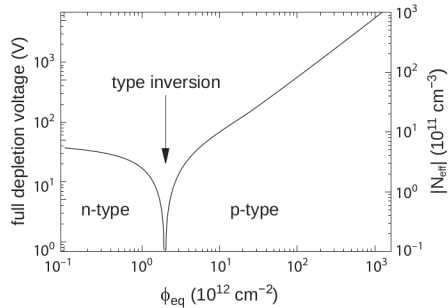
568 **DUE PAROLE IN PIÙ SUL SURFACE DAMAGE** A charge accumulation in oxide ( $SiO_2$ ) can  
 569 cause the generation of parasitic current with an obvious increase of the 1/f noise. Surface damages  
 570 are mostly less relevant than the previous one, since with the development of microelectronics and  
 571 with the miniaturization of components (in electronic industry 6-7 nm transistors are already used,  
 572 while for MAPS the dimensions of components is around 180 nm) the quantity of oxide in circuit  
 573 is reduced.

574 Let's spend instead two more other words on the more-relevant substrate damages: the general  
 575 result of high radiation level is the creation of new energy levels within the silicon band gap and  
 576 depending on their energy-location their effect can be different, as described in the Shockely-Read-  
 577 Hall (SRH) statistical model. The three main consequence of radiation damages are the changing  
 578 of the effect doping concentration, the leakage current and the increasing of trapping probability.

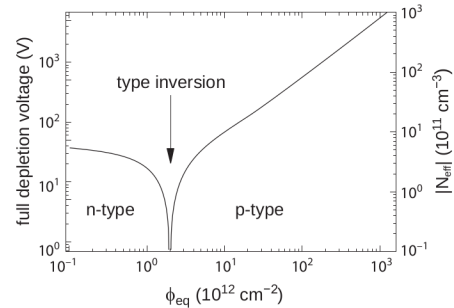
579 **Changing of the effective doping concentration:** is associated with the creation/removal  
 580 of donors and acceptors center which trap respectively electrons/holes from the conduction band  
 581 and cause a change in effective space charge density. Even an inversion (p-type becomes n-type<sup>1</sup>)  
 582 can happen: indeed it is quite common at not too high fluences ( $\phi_{eq} 10^{12-13} n_{eq} cm^{-2}$ ). A changing  
 583 in the doping concentration requires an adjustment of the biasing of the sensor during its lifetime  
 584 (eq.2.1) and sometimes can be difficult keeping to fully deplete the bulk.

---

<sup>1</sup>L'INVERSIONE OPPOSTA NON CE L'HA PERCHÈ?



(a) 1a



(b) 1b

585       **Leakage current:** is associated with the generation-recombination centers. It has a strong  
586 dependence with the temperature ( $I_{leak} \propto T^2$ ), whose solution is therefore to operate at lower  
587 temperature.

588       **Increase of trapping probability:** since the trapping probability is constant in the depleted  
589 region, the collected charge decreases exponentially with the drift path. The exponential coefficient,  
590 that is the mean trapping path, decreases after irradiation and typical values are 125-250  $\mu m$  and  
591 must be compared with the thickness of the depleted region which () corresponds to the mean drift  
592 path.

593       Different choices for substrate resistivity, for junctions type and for detector design are typically  
594 made to fight radiation issues. Some material with high oxygen concentration (as crystal produced  
595 using Czochralki (Cz) or float-zone (Fz) process (**CONTROLLA LA DIFFERENZA TRA I DUE**))  
596 for example, show a compensation effect for radiation damage; another example is the usage of  
597 n+ -in-p/n sensors (even if p+ -in-n sensors are easier and cheaper to obtain) to get advantage  
598 of inversion/to have not the inversion (since they are already p-type). After inversion the n+p  
599 boundary, coming from n+ in-n, but to keep using the sensor the depletion zone still must be  
600 placed near the diode.

# 601 Appendix B

## 602 FLASH radiotherapy

603 La radioterapia si usa nel 60 per cento dei pazienti, sia come cura che come trattamento palliativo.  
604 Si associa spesso ad altre cure e si può fare prima/durante/dopo un intervento.

605  
606 Si può fare in modi diversi: da dentro (brachytherapy) oppure da fuori (quella standard). Un  
607 requisito importante è la delinazione del target (non vuoi rischiare di beccare i tessuti sani), per  
608 cui prima tipicamente si fanno esami di imaginig del tumore. Tipicamente anche gli acceleratori  
609 stessi per la terapia sono provvisti di radiografia.

610 Un problema dei fotoni ad esempio è che il loro rilascio di dose è lineare, per cui danneggia  
611 anche i tessuti sani. Il problema dei protoni invece è che hanno un picco troppo stretto per cui non  
612 puoi coprire grosse zone e soprattutto se sbagli rischi davvero di danneggiare molto i tessuti sani.

### 614 B.1 Cell survival curves

615 Curva di efficacia del trattamento in funzione della dose:

$$\frac{S(D)}{S(0)} = e^{-F(D)} \quad (\text{B.1})$$

616 dove  $F(D)$

$$F(D) = \alpha D + \beta D^2 \quad (\text{B.2})$$

617 dove  $\alpha$  e  $\beta$  rappresentano due tipi di danno diversi: coefficients, experimentally determined, char-  
618 acterizing the radiation response of cells. In particular, alpha represents the rate of cell killing by  
619 single ionizing events, while beta indicates the maximal rate of cell killing by double hits observed  
620 when the repair mechanisms do not activate during the radiation exposure. Si ottiene una curva  
621 di sopravvivenza dove si vede la possibilità delle cellule di autoripararsi. A basse dosi infatti le  
622 cellule possono ripararsi.

623  
624 Per introdurre l'effetto FLASH introduco prima la therapeutic window.

625  
626 TCP è la tumor control Probability che indica la probabilità delle cellule del tumore di essere  
627 uccise dopo una certa dose (con in riferimento a dose in acqua)

628 Se una media di  $\mu(D)$  di cellule di tumore are killed con una dose D, la probabilità che n cellule  
629 sopravvivono è data da  $P(n|\mu)$  poisson:

$$P(n|\mu) = \frac{\mu(D)^n e^{-\mu(D)}}{n!} \quad (\text{B.3})$$

$$TPC(D) = P(n=0|\mu(D)) = e^{-\mu(D)} \quad (\text{B.4})$$

630 D'altra parte hai una probabilità di fare danno su normal tissue NTCP Normal Tissue Complica-  
631 tion Probability, che rappresenta il problema principale e che limita la massima radiazione erogabile  
632 Una scelta bilanciata si applica guardando a questi due fattori; si usa il therapeutic index definito  
633 come TCP/NTCP.

634 La cosa ottimale è ampliare la finestra del therapeutic ratio.

635  
636 CONV-RT 0.01-5 Gy/min. A typical RT regime today consists of daily fractions of 1.5 to 3  
637 Gy given over several weeks.

638 Nell Intra operative radiation therapy (IORT), where they reach values respectively about 20 and  
639 100 times greater than those of conventional radiation therapy.

640 FLASH vuole ultrahigh mean dose-rate (maggione di 40 Gy/s) in modo da ridurere anche il  
641 trattamento a meno di un secondo.

642

## 643 **B.2 FLASH effect**

644 Ci sono due effetti che affect the flsh effect and la sua applicabilità: Dose rate effect e oxygen

645  
646 Cellule che esibiscono hypoxia (cioè cellule che non hanno ossigeno sono radioresistenti); al  
647 contrario normoxia e physoxia non lo sono. la presenza di ossigeno rende la curva steeper indicando  
648 che lo stesso danno si raggiunge a livelli di dose più bassi rispetto al caso senza ossigeno.

649 FIGURA con una curva a confronto con e senza ossigeno.

650 Typically, the OER is in the order of 2.5–3.5 for most cellular systems

651 Quindi si vogliono sfruttare questi effetti per diminuire la tossicità sui tessuti sani

652

# 653 Bibliography

- 654 [1] W. Snoeys et al. “A process modification for CMOS monolithic active pixel sensors for  
655 enhanced depletion, timing performance and radiation tolerance”. In: (2017). DOI: <https://doi.org/10.1016/j.nima.2017.07.046>.
- 656 [2] D. Kim et al. “Front end optimization for the monolithic active pixel sensor of the ALICE  
657 Inner Tracking System upgrade”. In: *JINST* (2016). DOI: doi:10.1088/1748-0221/11/02/  
659 C02042.
- 660 [3] H. Kolanoski and N. Wermes. *Particle Detectors: Fundamentals and Applications*. OXFORD  
661 University Press, 2020. ISBN: 9780198520115.
- 662 [4] E. Mandelli. “Digital Column Readout Architecture for the ATLAS Pixel 0.25 um Front End  
663 IC”. In: (2002).
- 664 [5] M. Garcia-Sciveres and N. Wermes. “A review of advances in pixel detectors for experiments  
665 with high rate and radiation”. In: (2018). DOI: <https://doi.org/10.1088/1361-6633/aab064>.
- 666 [6] M. Dyndal et al. “Mini-MALTA: Radiation hard pixel designs for small-electrode monolithic  
667 CMOS sensors for the High Luminosity LHC”. In: (2019). DOI: <https://doi.org/10.1088/1748-0221/15/02/p02005>.
- 668 [7] M. Barbero. “Radiation hard DMAPS pixel sensors in 150 nm CMOS technology for opera-  
669 tion at LHC”. In: (2020). DOI: <https://doi.org/10.1088/1748-0221/15/05/p05013>.
- 670 [8] K. Moustakas et al. “CMOS Monolithic Pixel Sensors based on the Column-Drain Architec-  
671 ture for the HL-LHC Upgrade”. In: (2018). DOI: <https://doi.org/10.1016/j.nima.2018.09.100>.
- 672 [9] L. Pancheri et al. “A 110 nm CMOS process for fully-depleted pixel sensors”. In: (2019). DOI:  
673 <https://doi.org/10.1088/1748-0221/14/06/c06016>.
- 674 [10] L. Pancheri et al. “Fully Depleted MAPS in 110-nm CMOS Process With 100–300-um Active  
675 Substrate”. In: (2020). DOI: 10.1109/TED.2020.2985639.